A measurement of the polarizability of sodium clusters

G. Tikhonov, V. Kasperovich, K. Wong, and V. V. Kresin
Department of Physics and Astronomy, University of Southern California, Los Angeles, California 90089-0484
(Received 4 May 2000; published 6 November 2001)

The static electric dipole polarizabilities of sodium clusters Na_n for a series of sizes in the range $7 \leqslant n \leqslant 93$ were measured by electric field deflection of a supersonic cluster beam. Results for the smaller clusters are in overall good agreement with previous experiments. Polarizabilities of the larger clusters continue the downward trend with increasing size, but remain considerably above the bulk limit. There is a degree of correlation between the polarizability values and electronic shell structure. Furthermore, there is an indication that the polarizability is sensitive to the source conditions, possibly reflecting the influence of internal cluster temperature.

DOI: 10.1103/PhysRevA.64.063202 PACS number(s): 36.40.Cg, 73.22.−f

Alkali-metal clusters appear to be among the most polarizable particles in existence. With n mobile valence electrons delocalized over an ionic framework of radius R_n, the static electric polarizability has been parametrized as $\alpha_n \approx (R_n + \delta)^3$ [1]. For a neutral spherical cluster with closed electronic shells, the radius is $R_n = r_s n^{1/3}$ and δ is a measure of the electron spill-out beyond the ionic boundary (for sodium, the Wigner-Seitz radius is $r_s \approx 2.1$ Å and $\delta \approx 1.3$ Å; see below). Thus α_n exceeds even the textbook value $\alpha = R^3$ for an ideal conducting sphere.

Since the pioneering measurement by Knight *et al.* [2], which followed shortly after their discovery of electronic shell structure in alkali-metal clusters [3], sodium cluster polarizabilities have continued to attract attention as a benchmark of our comprehension of the structure and electromagnetic response of a nanoscale size-quantized system. They also have important manifestations in a variety of strong long-range attractive interactions [4]. The original measurement, which covered the range of $Na_{n=2-40}$, has been essentially confirmed by a recent experiment on $Na_{n=2-21}$ [5] and by a detailed study of alkali-metal dimer polarizabilities [6]. It was also found to be consistent with Na_n^+ polarizabilities derived from the oscillator strength moments of ion photoabsorption spectra [7]. Other recent metal cluster polarizability measurements include those on Al_n [8], Li_n [5], Na_nLi_m [9], and Ni_n [10].

A remarkably large number of theoretical calculations based on various methodologies have been directed at this quantity (see, e.g., the overview in [11], and [12–14] and references therein). By and large, theory tends to underestimate the experimentally measured values. Different corrections have been proposed to deal with this long-standing discrepancy, but the situation remains unresolved. For example, recent theoretical work has addressed the possibility of a strong influence of metal cluster temperature on the electric polarizability [12–16]. In fact, this idea was mentioned even in the original experimental paper [2]; however, it still awaits a definitive experimental answer. Note that the polarizabilities of several Ga_nAs_m and Ge_nTe_m clusters have been found to vary strongly with temperature [17].

To understand the behavior of cluster polarizability and its evolution toward the bulk limit, it is useful to extend the range of the experimentally measured values. In this paper, we report on a measurement of Na_n static electric polarizabilities for selected cluster sizes in the interval $7 \leqslant n \leqslant 93$. We compare the values with previous experiments and discuss the trends observed for the larger clusters. We also show some evidence for the sensitivity of the polarizability to the cluster source conditions.

The size-dependent polarizabilities of free neutral clusters are measured by deflecting a collimated cluster beam in an inhomogeneous electric field. An outline of the experiment is shown in Fig. 1. The sodium clusters are produced by a supersonic cluster source (vapor temperature 873 K, argon carrier gas pressure 600–620 kPa, nozzle diameter 75 μm, and temperature 1093 K). The resulting beam is collimated by two round skimmers with diameters of 0.4 mm and 1.5 mm (8 and 178 mm from the nozzle, respectively). This double skimmer scheme defines the beam geometry and counteracts any beam widening which may be caused by cluster scattering off the background gas present at relatively high pressure downstream from the expansion. Approximately 45 cm past the second skimmer, the beam is collimated to a rectangular cross section of 0.25 mm $\times$ 0.76 mm and enters the deflection field region. The inhomogeneous ''two-wire'' electric field [18] is produced by applying high voltage to a pair of curved (curvature radius 2.4 mm for both) deflection plates spaced by 2.4 mm [19]. These 15 cm long plates are machined out of aluminum, polished, and electropolished. A voltage of 30 kV is applied across the gap with no detected leakage current.

Following a 110 cm flight path from the deflection field region exit, the cluster beam enters the detector through a 0.64 mm wide movable collimating slit. The clusters are ionized by a filtered UV lamp, mass selected by a quadrupole mass analyzer (QMA), and detected by an ion counter which utilizes a high-voltage dynode. The cluster beam is alternately chopped by two fast 50% mechanical choppers spaced by 130 cm (see below). The resulting time-varying signal from the ion detector is recorded by a multichannel scaler (MCS). A computer controls and repeatedly monitors the deflection plate voltage, governs the detector collimating slit movement, performs mass selection by means of the QMA, and stores data collected by the MCS.

With the experimental parameters described above, the deflected cluster beam profile at the detector entrance is typi-

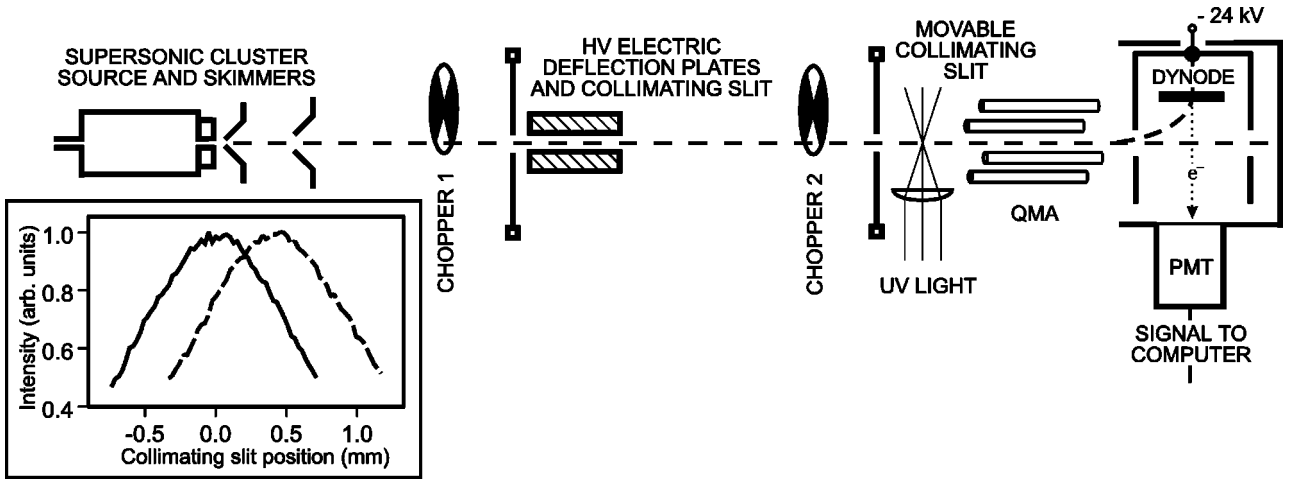

FIG. 1. Top view of the experimental arrangement (not to scale). A collimated supersonic beam of sodium clusters is deflected by an inhomogeneous electric field. With the help of two high-speed chopper wheels, the beam deflection profile and its velocity distribution are measured simultaneously. PMT is a photomultiplier tube covered by a scintillator. Inset: An undeflected (solid line) and deflected (dashed line) profile of the Na_8 signal.

cally shifted by ≈ 0.5 mm with respect to the zero-field beam profile. The two-wire field deflects a Na_n cluster by an amount (see, e.g., [2])

$$d = \frac{\alpha_{cl}}{n} \frac{C}{m_{\mathrm{Na}}} \frac{V^2}{v^2} \tag{1}$$

where α_{cl} is the rotationally averaged static electric dipole polarizability. Here m_{Na} is the mass of a sodium atom, C is a factor defined by the deflection plate geometry and apparatus dimensions, V is the plate voltage, and v is the cluster velocity. As in previous experiments [2,5], our measured polarizabilities are referenced to one fixed cluster polarizability measured on the same apparatus within the same experimental run. This eliminates the imprecisely known geometrical factor C from consideration. In our case, a conveniently stable reference cluster was Na_8, whose absolute polarizability was subsequently calibrated against the well-established value for Na_2 [2,5,6].

In a real experiment, one measures the deflection not of a single cluster, but of a supersonic beam which possesses a finite geometrical width and a certain velocity distribution. Furthermore, cluster source intensity tends to fluctuate over the course of the experiment. All these factors can broaden, if not downright distort, the deflection profile of the cluster beam. As a consequence, we devoted significant effort to controlling them. A detailed description of our treatment of velocity distribution and beam width effects will be presented elsewhere [20]. In particular, it can be shown that for the present experiment Eq. (1) remains quite accurate if d is taken to represent the displacement of the beam profile maximum and $1/v^2$ is replaced by $\langle 1/v^2 \rangle$, i.e., averaged over the beam velocity distribution.

The main source of experimental error is the uncertainty in the position of the beam profile maximum. The beam profile for a particular cluster is mapped out by setting the QMA to the chosen mass and measuring the counting rate for various positions of the movable detector entrance slit. (More precisely, at each slit position the rates for several cluster sizes are collected by switching the QMA between several settings.) The results were normalized to the detector sensitivity curve [21]. Unfortunately, all the intensity measurements require a significant interval of time, while cluster production rates in the supersonic source have a tendency to fluctuate over this interval. To eliminate any systematic influence of these fluctuations on the beam profile, we randomize the order in which the collimating slit covers its specified set of 60 positions. Furthermore, by reducing the measurement time for each collimator position we also reduce the statistical impact of the source production rate instabilities. This reduction is made up for by scanning the complete beam profile several times and adding up the results. Specifically, for both deflected and undeflected beam profiles the detector collimator usually made between four and sixteen passes across the beam profile, each lasting between seven and twenty minutes. The inset in Fig. 1 shows typical deflected and zero-field cluster beam profiles obtained by means of this random-sequence multipass scan technique. Please note that these profiles represent actual experimental data and have not been subjected to smoothing or other statistical treatment. The position of the beam profile maximum is determined by a least-squares fit to a parabola [22]. Despite the robustness of the profile mapping method, source fluctuations become more serious for the larger clusters and result in greater uncertainties in the measured polarizabilities.

The other critical variable in Eq. (1) is the beam velocity distribution. Customarily, this distribution is analyzed only before and after a deflection measurement. However, in this case the aforementioned cluster beam drifts and fluctuations may become a source of error. In order to combat it, we always measure the beam deflection and the velocity distribution *simultaneously*. As shown in Fig. 1, the spatial profiles of the cluster beam are measured while it is being

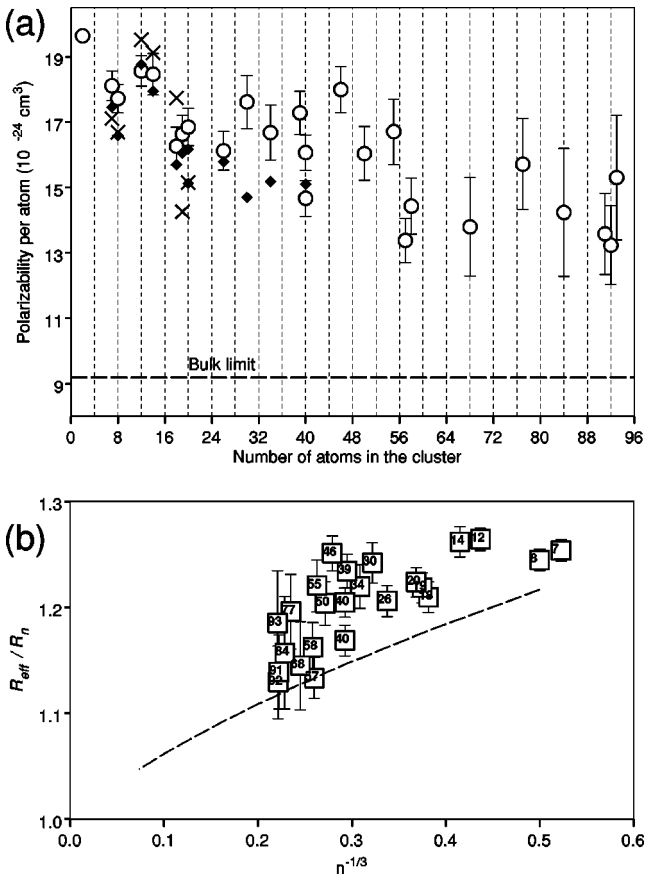

FIG. 2. Static dipole polarizabilities of Na_n clusters. (a) Polarizability per atom with Na_2 serving as the reference cluster. Circles, this work; diamonds, Ref. [2]; crosses, Ref. [5]. The estimated error bars are shown only for the present experiment. The horizontal line depicts the classical limit for a sodium sphere (see text). (b) Polarizabilities expressed in terms of the classical limit: the effective radius is defined as $\alpha_n \equiv R_{eff}^3$, and R_n is the core radius. For the common parametrization $R_{eff} \approx (R_n + \delta)$, a fit yields $\delta = 1.3$ Å. The dashed line is a plot of the analytical formula [26] derived within the surface-plasma-pole approximation of linear response theory.

chopped by one of the pair of mechanical choppers. Thus for every collimating slit position we acquire a complete time-of-flight profile. (The detector and electronics time-delay uncertainty is excluded by combining signals from the two choppers [23,24]. Furthermore, each chopper is used in both clockwise and counterclockwise rotation, eliminating possible errors associated with alignment and synchronization asymmetries.) We developed a method that allows us to extract the cluster beam velocity distribution directly from such time-of-flight profiles without having to fit any model distributions [20]. This approach yields average velocity values with an estimated accuracy of 0.2% to 0.4%. It even allowed us to marginally resolve velocity differences within one deflected beam profile: according to Eq. (1), slower clusters will tend to undergo a slightly greater deflection [20]. In summary, then, only a fairly small part of the overall experimental error derives from the beam velocity measurement.

Our values for the rotationally averaged dipole polarizabilities are plotted in Fig. 2 and listed in Table I. The error bars are derived from the standard deviations in the measurement of d, v, and V [see Eq. (1)], and the variations in the literature value of α_{Na_2} [2,5,6]. Numerically, this results in a systematic contribution of $\approx 2.5\%$ error (in quadrature) deriving from calibrating the polarizabilities against a fixed reference cluster; the remainder of each error bar comes from size-dependent experimental uncertainties.

TABLE I. Mean polarizabilities of sodium clusters. The absolute values were obtained by scaling the deflection data to the polarizability of Na_2, whose average literature value [2,5,6] is listed in the first line.

Number of atoms	Polarizability per atom (Å^3)
2	19.6
7	18.1 ± 0.5
8	17.7 ± 0.4
12	18.6 ± 0.5
14	18.5 ± 0.6
18	16.3 ± 0.6
19	16.6 ± 0.6
20	16.8 ± 0.6
26	16.1 ± 0.6
30	17.6 ± 0.8
34	16.7 ± 0.8
39	17.3 ± 0.7
40	14.7 ± 0.5
40	16.1 ± 0.5
46	18.0 ± 0.7
50	16.0 ± 0.8
55	16.7 ± 1.0
57	13.4 ± 0.7
58	14.4 ± 0.9
68	13.8 ± 1.5
77	15.7 ± 1.4
84	14.2 ± 2.0
91	13.6 ± 1.2
92	13.2 ± 1.2
93	15.3 ± 1.9

Figure 2(a) also includes the results of previous experimental studies for comparison. As mentioned above, the data in [2] and [5] are available for sizes up to Na_{40} and Na_{21}, respectively. There is, generally, a good agreement within the stated uncertainty limits [25], although a few larger deviations are also found. The polarizabilities for sizes up to Na_{93} reported here continue the previously established downward trend; see Fig. 2(b) [26]. However, they remain substantially above the bulk limit. In agreement with the prior measurements, some correlation between polarizabilities and shell structure is evident for the larger cluster sizes as well. Commonly, magic-number sodium clusters display lower polarizabilities than their nearest neighbors. Nevertheless, in some cases there is no one-to-one correspondence between the patterns of polarizability values and of shell closings in the sodium cluster mass spectra. This is especially apparent in

the Na_{18} to Na_{20} polarizability alternation, where our data almost precisely follow the results of [2]. Likewise, in the Na_{57}-Na_{58} sequence no drop is evident.

The data for all cluster sizes are consistent in terms of exceeding most ground-state theoretical values, as mentioned in the Introduction. This once again raises the question of the possible importance of cluster temperature and isomerism effects. Similar effects, associated with variations in source expansion conditions, could also account for the discrepancies among the data sets of different groups.

In this respect, it is noteworthy that in two separate measurements we obtained two somewhat different values for the Na_{40} polarizability. It may be not coincidental that the supersonic expansion conditions in the two runs, while similar, produced nonidentical mass spectral distributions, as shown in Fig. 3. Interestingly, Clemenger *et al.* [2,19] also reported two separate values for the polarizability of Na_{20} obtained under different source conditions. As can be seen from Fig. 2(a), the upper value is in very good agreement with our data, while the lower value is very close to that measured by Rayane *et al.* [5]. It is not yet clear what lies at the root of such variations, but note that evaporative ensemble theory [27,28] predicts that each cluster size in the supersonic beam possesses a relatively wide temperature distribution. Even though the originally hot clusters undergo a rapid in-flight evaporation stage, the shape, or skewness, of the resulting temperature distribution should retain a memory of the initial condensation envelope. Therefore, if the polarizability is indeed a sensitive function of the internal particle temperature, the ensemble-averaged value will vary with the source expansion conditions. Thus relatively small shifts of cluster polarizabilities may harbor important information about structural and thermal dynamics.

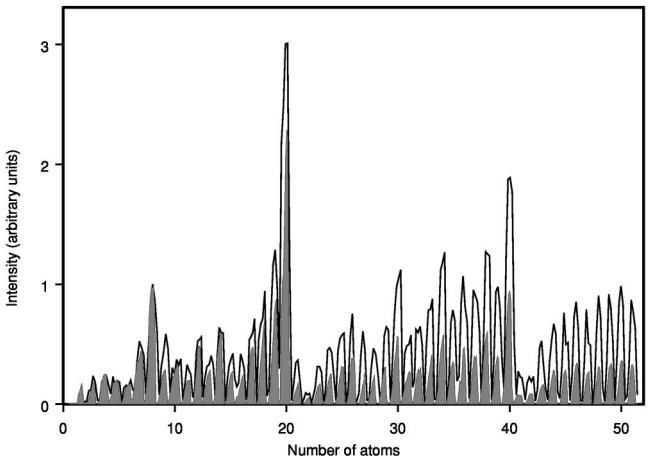

FIG. 3. Cluster abundance spectra acquired during runs that produced two distinct values of the Na_{40} polarizability. The shaded and solid-line spectra correspond to the higher and lower values of α_{40}, respectively.

We would like to thank K. Hansen and P. Brockhaus for very useful discussions, and the staff of the USC Natural Sciences Machine Shop for expert technical help. This work was supported by the National Science Foundation under Grant No. PHY-9600039.

[1] W. A. de Heer, W. D. Knight, M. Y. Chou, and M. L. Cohen, in *Solid State Physics*, edited by H. Ehrenreich and D. Turnbull (Academic, New York, 1987); Vol. 40.
[2] W. D. Knight, K. Clemenger, W. A. de Heer, and W. A. Saunders, Phys. Rev. B **31**, 2539 (1985).
[3] W. D. Knight, K. Clemenger, W. A. de Heer, W. A. Saunders, M. Y. Chou, and M. L. Cohen, Phys. Rev. Lett. **52**, 2141 (1984).
[4] V. V. Kresin and C. Guet, Philos. Mag. B **79**, 1401 (1999).
[5] D. Rayane, A. R. Allouche, E. Benichou, R. Antoine, M. Aubert-Frecon, Ph. Dugourd, M. Broyer, C. Ristori, F. Chandezon, B. A. Huber, and C. Guet, Eur. Phys. J. D **9**, 243 (1999).
[6] V. Tarnovsky, M. Bunimovicz, L. Vušković, B. Stumpf, and B. Bederson, J. Chem. Phys. **98**, 3894 (1993).
[7] M. Schmidt and H. Haberland, Eur. Phys. J. D **6**, 109 (1999).
[8] W. A. de Heer, P. Milani, and A. Châtelain, Phys. Rev. Lett. **63**, 2834 (1989).
[9] R. Antoine, D. Rayane, A. R. Allouche, M. Aubert-Frécon, E. Benichou, F. W. Dalby, Ph. Dugourd, and M. Broyer, J. Chem. Phys. **110**, 5568 (1999).
[10] M. B. Knickelbein, J. Chem. Phys. **115**, 5957 (2001).
[11] K. D. Bonin and V. V. Kresin, *Electric-Dipole Polarizabilities of Atoms, Molecules and Clusters* (World Scientific, Singapore, 1997).
[12] S. Kümmel, J. Akola, and M. Manninen, Phys. Rev. Lett. **84**, 3827 (2000).
[13] S. A. Blundell, C. Guet, and R. R. Zope, Phys. Rev. Lett. **84**, 4826 (2000).
[14] L. Kronik, I. Vasiliev, and J. R. Chelikowsky, Phys. Rev. B **62**, 9992 (2000).
[15] A. Bulgac and C. Lewenkopf, Europhys. Lett. **31**, 519 (1995).
[16] W. Müller and W. Meyer, J. Chem. Phys. **85**, 953 (1986).
[17] R. Schäfer, S. Schlecht, J. Woenckhaus, and J. A. Becker, Phys. Rev. Lett. **76**, 471 (1996).
[18] N. F. Ramsey, *Molecular Beams* (Oxford University Press, New York, 1956).
[19] K. Clemenger, Ph.D. dissertation, University of California, Berkeley, 1985.
[20] G. Tikhonov, K. Wong, V. Kasperovich, and V. V. Kresin (unpublished).
[21] The detector sensitivity profile depends mostly on the probability of cluster ionization by UV light and on the ability of ion optics to steer the ion into the QMA. The ionization probability is related to light focusing and to the internal properties of the cluster, while ion optics performance is influenced by the mass. As a result, the detector sensitivity curve is generally cluster size dependent. It was measured individually for each cluster size.
[22] P. R. Bevington, *Data Reduction and Error Analysis for the*

Physical Sciences (McGraw-Hill, New York, 1969).
[23] V. V. Kresin, V. Kasperovich, G. Tikhonov, and K. Wong, Phys. Rev. A **57**, 383 (1998).
[24] M. Vollmer, K. Selby, V. Kresin, J. Masui, M. Kruger, and W. Knight, Rev. Sci. Instrum. **59**, 1965 (1988).
[25] Results of [2] are available as a table in Ref. [19].
[26] V. V. Kresin, Phys. Rep. **220**, 1 (1992).
[27] K. Hansen and U. Näher, Phys. Rev. A **60**, 1240 (1999).
[28] S. Bjørnholm, and J. Borggreen, Philos. Mag. B **79**, 1321 (1999).